Article citation info:
BOŠNJAK S, GNJATOVIĆ N, MILENOVIĆ I. From 'a priori' to 'a posteriori' static stability of the slewing superstructure of a bucket wheel excavator. Eksploatacja i Niezawodnosc – Maintenance and Reliability 2018; 20 (2): 190–206, http://dx.doi.org/10.17531/ein.2018.2.04.

Srđan BOŠNJAK
Nebojša GNJATOVIĆ
Ivan MILENOVIĆ

FROM 'A PRIORI' TO 'A POSTERIORI' STATIC STABILITY OF THE SLEWING SUPERSTRUCTURE OF A BUCKET WHEEL EXCAVATOR

RÓWNOWAGA STATYCZNA NADWOZIA OBROTOWEGO KOPARKI KOŁOWEJ: OD MODELU "A PRIORI" DO MODELU "A POSTERIORI"

The complexity of the slewing superstructure (SS) balancing problem derives from the changeability of its geometric configuration, the complexity of working conditions as well as multiple limitations of the possible set of solutions. Having in mind the fact that the existing reference literature does not fully specify the procedure of static stability proof, the aforementioned procedure is presented in detail for the first time in this paper. A major contribution is represented in the classification of the slewing superstructure models into two groups which were named: the 'a priori' model (designed image of the SS) and the 'a posteriori' model (actual image of the SS). The fundamental stages of the 'a posteriori' model development method are presented in the paper. The transformation and validation of the calculation model 'a priori' to the calculation model 'a posteriori' was conducted on the basis of weighing results. A calculation of the basic parameters of the bucket wheel excavator (BWE) superstructure was conducted for both analyzed models by using the in-house developed software. The 'a posteriori' models provide a reliable calculation of the SS static stability and may be used not only for static stability proof of the machine as a whole, but also for load analysis of substructures and elements of BWE and related surface mining machines, such as spreaders. Besides that, the previously mentioned models are of extreme importance for a successful and reliable exploitation and maintenence of the machine since they present the basis for adjustment and control of limiting winch rope forces values, periodic control of mass and center of gravity position, as well as for a possible reconstruction which would be conducted in order to realize better customization of the machine versus operating conditions.

***Keywords**: bucket wheel excavator, slewing superstructure, static stability proof.*

Złożoność problematyki stabilizacji nadwozia obrotowego (slewing superstructure, SS) wynika ze zmienności jego konfiguracji geometrycznej, złożoności warunków pracy oraz wielu ograniczeń możliwego zbioru rozwiązań. Ponieważ istniejąca literatura nie opisuje w pełni procedury przeprowadzania dowodu na równowagę statyczną, niniejsza praca stanowi pierwszą próbę opracowania takiej procedury. Głównym wkładem niniejszego artykułu jest klasyfikacja modeli nadwozia obrotowego na dwie grupy: model "a priori" (zaprojektowany obraz SS) i model "a posteriori" (rzeczywisty obraz SS). W artykule przedstawiono podstawowe etapy metody opracowywania modelu "a posteriori". Walidacji modelu obliczeniowego "a priori" i jego transformacji do modelu obliczeniowego "a posteriori" dokonano na podstawie wyników ważenia. Dla obydwu analizowanych modeli wykonano obliczenia podstawowych parametrów nadwozia koparki kołowej przy użyciu oprogramowania własnego. Modele "a posteriori" zapewniają niezawodne obliczenia równowagi statycznej SS i mogą być stosowane nie tylko do sprawdzania równowagi statycznej maszyny jako całości, ale również do analizy obciążenia podzespołów i elementów koparki kołowej oraz powiązanych maszyn górniczych, takich jak zwałowarki. Poza tym wspomniane wcześniej modele mają ogromne znaczenie dla skutecznej i niezawodnej eksploatacji i konserwacji maszyn, ponieważ stanowią podstawę do regulacji i kontroli granicznych wartości sił liny wciągarki, okresowej kontroli masy i położenia środka ciężkości, jak również możliwej rekonstrukcji, którą przeprowadza się w celu lepszego dostosowania maszyny do warunków pracy.

***Słowa kluczowe**: koparka kołowa, nadwozie obrotowe, równowaga statyczna.*

1. Introduction

Identifying the weight and the centre of gravity (COG) position i.e. the basic parameters of static stability (BPSS) is of extreme importance during the development of bucket wheel excavators (BWEs) projects, as well as during their exploitation and maintenance [5]. This is the reason why validation of the BPSS calculation values is performed by weighing, conducted immediately after the first BWE erection and also after every reconstruction of the slewing superstructure (SS) [1,9,11,12].

The weight of the bucket wheel boom subsystem is dominantly influencing the intensity of the load of its hanging system i.e. winch rope forces [5]. Additionally, the SS COG position has a major influence on the load of the slew bearing [16,17]. According to the presented facts, it can be concluded that precise identification of BPSS enables: (a) a reliable adjustment of the winch rope forces limiting values, which present basic protection against the SS static stability loss, (b) an identification of the loads of the catch hooks, which prevent loss of the static stability in extreme load cases and (c) a determination of unevenness of slew bearing rolling bodies load distribution.

In reference literature in the field of bucket wheel excavators [9,15] – the problem of static stability is analyzed only in general. The influence of the BPSS on the loads of the bucket wheel boom stays is analyzed in [5], while the influence of counterweight (CW) and bucket wheel (BW) with drive mass on the dynamic response of the SS is analyzed in paper [4]. Dynamics of the large-scale load-carrying

structures is especially influenced by the slewing superstructure COG position [13,14].

The complexity of the SS static stability proof arises from the changeability of its geometric configuration and a relatively large number of partial loads combinations. In the literature which was available to the authors, only the calculation of the safety factor against overturning on the basis of project documentation i.e. before weighing (‘a priori’) is analyzed. Furthermore, such calculation is provided scarcely and in general. Also, the calculation algorithm with appropriate expressions is not given. The investigations, published in research papers [1,11,12], are entirely dedicated to the problems of experimental determination of the SS weight and its COG position. The static stability proof conducted on the basis of BPSS obtained by weighing (‘a posteriori’) is not even mentioned. With these facts in mind, the procedure of the SS static stability proof ‘a priori’ is presented, and the original procedure of static stability proof ‘a posteriori’ is developed and fully included in this paper. Research presented in this paper is the sequel of the research published in [5] thus the object of analysis is the same: BWE 1600 (Fig. 1 in [5]). Development of the SS ‘a posteriori’ models is of extreme importance if perceived in the light of the fact that BWEs are machines designed for perennial exploitation in harsh working conditions. During their exploitation life, which for the BWEs operating in Serbian open-pit mines exceeds 40 years, reconstructions due to technological [2] or structural [2,6] failures, as well as failures of vital mechanisms [10], or executed in order to realise revitalization/modernization of excavating units [3,15], are inevitable. By nature, the mentioned reconstructions are dominantly executed on the SS responsible for the realisation of the excavation process, and inevitably followed by an experimental control of BPSS and the eventual correction of the CW mass before putting the excavator back to exploitation. The use of ‘a posteriori’ static stability proof procedure enables the determination of actual values of the factor of safety against overturning for the reconstructed SS. Besides, regardless of the cause (check out or reconstruction), the SS weighing procedure causes direct (engagement of specialists and specialized equipment) and indirect material losses due to the system standstill. For example, three days are needed for the realisation of SS weighing of the BWE which is a vital part of the overburden excavation system on the Tamnava East field open-pit mine (Serbia), whereby indirect costs caused by the system standstill are equal to 9232 €/h [7]. Three weighing procedures were conducted prior to putting the BWE 1600 to exploitation [5]. The use of the ‘a posteriori’ static stability proof procedure would enable the correction of the CW mass on the basis of two weighing procedures, thus essentially reducing the indirect losses, while fully providing the stability of the machine.

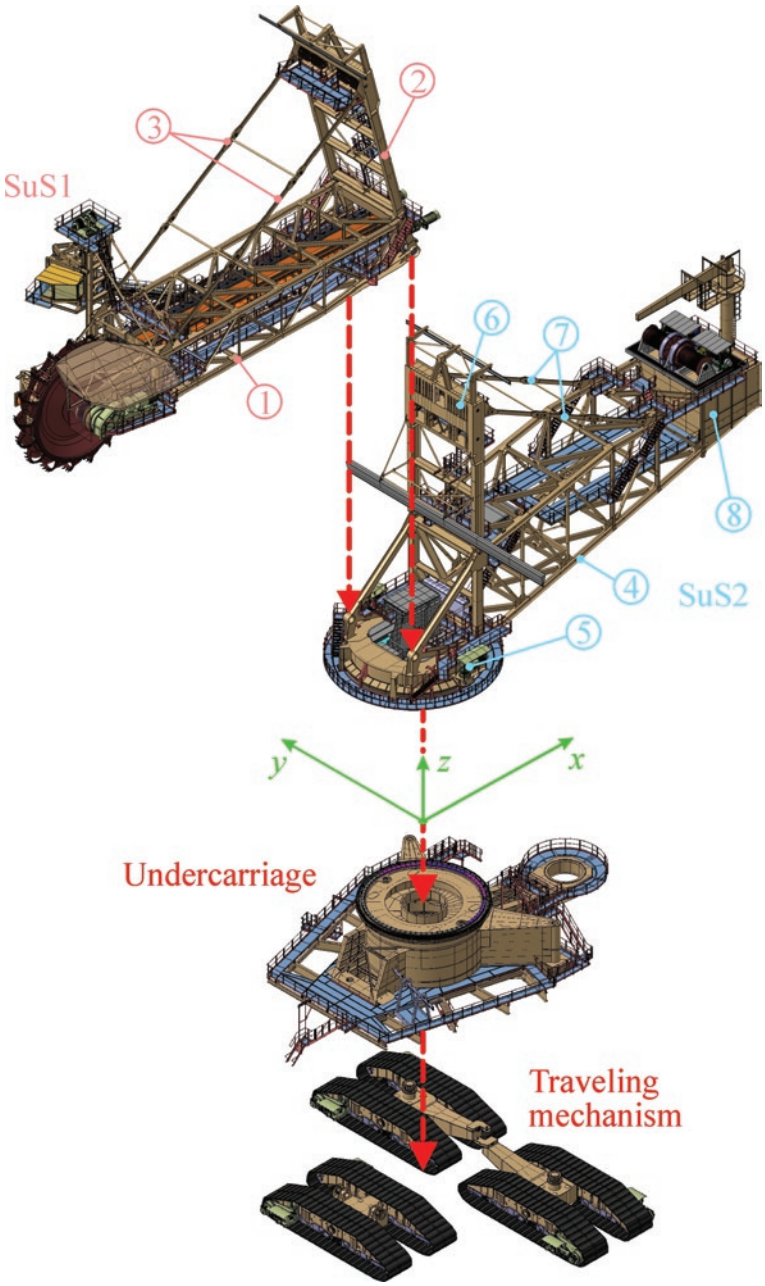

Fig. 1. Basic substructures of the BWE 1600: 1-bucket wheel boom; 2-mast 1; 3-bucket wheel boom stays; 4- counterweight boom; 5- slewing platform; 6-mast 2; 7-counterweight boom stays; 8- counterweight

The proposed static stability proof procedure ‘a posteriori’ has a wider significance because it can be successfully used when proving the static stability of spreaders and similar machines used in the systems for surface mining, as well as large-scale cranes.

2. Static stability of the slewing superstructure

The SS is leaning on the radiaxial slew bearing (RSB) which distributes the loads to the undercarriage and enables its slewing. For the static stability proof in the RSB plane, the following influences are accounted for:

- all of the loads acting upon substructure 1 (SuS1: bucket wheel boom (BWB)+mast 1 (M1)+BWB stays (BWBS), Fig. 1) and 2 (SuS2: counterweight boom (CWB) with slewing platform (SP)+mast 2 (M2)+CWB stays (CWBS), Fig. 1), as well as CW;
- ground reactions due to BW partial leaning;
- overload forces.

It is important to note that points of application of all the loads acting upon SuS1, in relation to the conditionally stationary coordinate system, are dependent of the BWB hoisting angle, which is not the case with loads acting upon SuS2.

The BWB hoisting mechanism of the BWE 1600 is not equipped with the system for continuous adjustment of winch rope forces extreme values. Their setting values (S_A: minimum - ‘’warning’’; S_{AA}: minimum - ‘’stop’’; S_Z: maximum - ‘’warning’’; S_{ZZ}: maximum - ‘’stop’’) remain constant on the complete domain of the BWB hoisting angle. The minimum and maximum rope force intensities ($S_{HZ3.1,min}$ and $S_{HZ3.1,max}$) obtained for load case (LC) HZ3.1 [8] (Tables 1 and

2) are representative for determining the winch rope forces setting values:

$$S_A = 0.94 S_{HZ3.1,min} \quad (1)$$

$$S_{AA} = 0.87 S_{HZ3.1,min} \quad (2)$$

$$S_Z = 1.08 S_{HZ3.1,max} \quad (3)$$

$$S_{ZZ} = 1.13 S_{HZ3.1,max} \quad (4)$$

Ground reactions caused by partial leaning of the BW and overload forces are determined for three characteristic LCs of the SuS1, Fig. 2:

- LC 1: dead load (G_{SuS1}=G_{BWB}+G_{M1}+G_{BWBS});
- LC 2: dead load (G_{SuS1}), weight of the material on belt conveyor 1 (F_1), incrustation of the BW (V_0) and conveyor 1 (V_1) and the digging force (U_F);
- LC 3: dead load (G_{SuS1}), weight of the material on belt conveyor 1 (F_1), incrustation of the BW (V_0) and conveyor 1 (V_1) and the digging force (U_L).

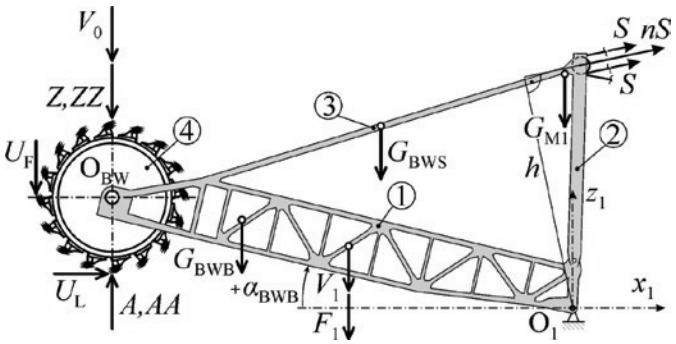

Fig. 2. The scheme for calculating the ground reaction due to partial leaning of the BW and overload forces: 1-BWB; 2-M1, 3-BWBS; 4-BW; S-winch rope force; n-number of rope legs; h-moment arm of pulley force; A, AA-ground reactions; G_{BWB}, G_{M1}, G_{BWBS}-weights of BWB, M1, BWBS; F_1-weight of material on belt conveyor 1; O_{BW}-center of the BW; U_F=U_L- nominal tangential component of the digging force; V_0 and V_1-weight of BW and conveyor 1 incrustation; Z, ZZ-overload forces; α_{BWB}-BWB hoisting angle

In the mentioned LCs, intensities of ground reactions (A, AA) are calculated on the basis of setting values of minimum winch rope forces (S_A and S_{AA}, expressions (1) and (2)), using the moment equation for y_1 axis, Fig. 2:

$$M_{y1,i} = S_A nh + \sum_L Lx_{1,L} - A_i x_{1,OBW} = 0, \quad (5a)$$

$$M_{y1,i} = S_{AA} nh + \sum_L Lx_{1,L} - AA_i x_{1,OBW} = 0, \quad (5b)$$

where: for LC 1, i=1, L=G_{SUS1}; for LC 2, i=2, L=G_{SUS1},F_1,V_0,V_1,U_F; for LC 3, i=3, L=G_{SUS1},F_1,V_0,V_1,U_L.

Expressing A_i and AA_i from equations (5a and 5b) respectively, while taking into consideration that according to [4] the calculation intensity of ground reaction is increased by 10%, the following equations are obtained:

$$A_i = 1.1 \frac{nh}{x_{1,OBW}} \left(S_A + \sum_L \frac{Lx_{1,L}}{nh} \right) = 1.1 \frac{nh}{x_{1,OBW}} \left(S_A - \sum_L S_L \right), \quad (6a)$$

$$AA_i = 1.1 \frac{nh}{x_{1,OBW}} \left(S_{AA} + \sum_L \frac{Lx_{1,L}}{nh} \right) = 1.1 \frac{nh}{x_{1,OBW}} \left(S_{AA} - \sum_L S_L \right), \quad (6b)$$

where S_L is the intensity of winch rope force induced by the influence of corresponding partial loading.

The overload forces are obtained by an analogous procedure, where as the basis for calculation, setting values of maximum winch rope forces (S_Z and S_{ZZ}, expressions (3) and (4)) are adopted:

$$Z_i = 1.1 \frac{nh}{x_{1,OBW}} \left(S_Z + \sum_L \frac{Lx_{1,L}}{nh} \right) = 1.1 \frac{nh}{x_{1,OBW}} \left(S_Z - \sum_L S_L \right) \quad (7a)$$

$$ZZ_i = 1.1 \frac{nh}{x_{1,OBW}} \left(S_{ZZ} + \sum_L \frac{Lx_{1,L}}{nh} \right) = 1.1 \frac{nh}{x_{1,OBW}} \left(S_{ZZ} - \sum_L S_L \right). \quad (7b)$$

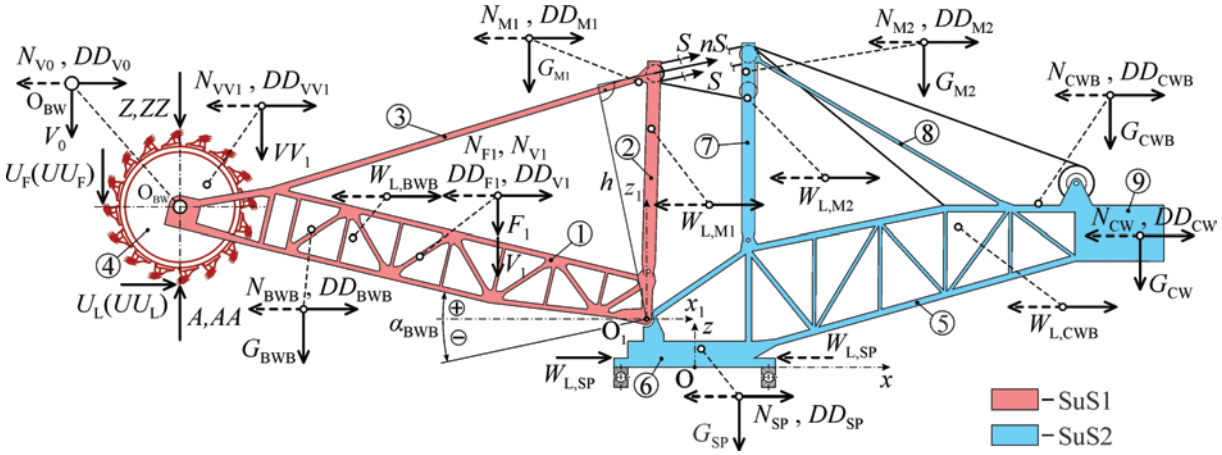

Fig. 3. The scheme of slewing superstructure loading: 1-BWB; 2-M1; 3-BWBS; 4-BW; 5-CWB; 6-SP; 7-M2; 8-CWBS; 9-CW; O_{BW}-center of the BW; S-winch rope force; n-number of rope legs; h-moment arm of the pulley force; G_{BWB}, G_{M1}, ..., G_{CW}-dead weights of substructures and CW; F_1-weight of material on belt conveyor 1; V_0 and V_1-weight of BW and conveyor 1 incrustation; VV_1-weight of the material in blocked BW chute; N_{BWB}, N_{M1}, ..., N_{CW}-longitudinal horizontal forces caused by normal inclination; NN_{BWB}, NN_{M1}, ..., NN_{CW}- longitudinal horizontal forces caused by transport inclination; $W_{L,BWB}$, $W_{L,M1}$, ..., $W_{L,CWBS}$-forces caused by longitudinal wind (in operation); $WW_{L,BWB}$, $WW_{L,M1}$, ..., $WW_{L,CWBS}$ -forces caused by longitudinal wind (out of operation); U_F=U_L-nominal tangential component of the digging force; UU_F=UU_L-maximum tangential component of the digging force; A, AA-ground reactions due to the partial leaning of the BW; Z, ZZ-overload forces; α_{BWB}-BWB hoisting angle; DD_{BWB}, DD_{M1}, ..., DD_{CW}-forces caused by earthquake

Table 1. Load combinations for BWS case

Loads	Load case[a]						
	H1.1	HZ3.1	HZ3.2	HZS4.4	HZS4.8	HZG5.3	HZG5.4
Group 1							
G	+	+	+	+	+	+	+
Group 2							
F_1	+	+	0	+	0	0	+
V_0	+	+	+	+	0	0	+
V_1	+	+	+	+	0	0	+
VV_1	0	0	0	+	0	0	0
W_L	0	$-x$[f]	0	$-x$	$-x$	$-x$	0
WW_L	0	0	$-x$	0	0	0	0
N[d]	$-x$	$-x$	$-x$	$-x$	$-x$	$-x$	$-x$
U_F	+	+	0	+	0	0	+
Z_1	0	0	0	0	+	0	0
ZZ_1	0	0	0	0	0	+	0
DD[e]	0	0	0	0	0	0	$-x$

[a]according to [8]; [b]sign "+" means that the load acts; [c]sign "0" means that the load does not act; [d]normal inclination (5%); [e]earthquake (11%); [f]load action caused by longitudinal wind, inclination and earthquake in "–x" direction (Fig. 3)

Table 2. Load combinations for CWS case

Loads	Load case[a]						
	H1.1	HZ3.1	HZ3.2	HZS4.1	HZS4.7	HZG5.2	HZG5.4
Group 1							
G	+	+	+	+	+	+	+
Group 2							
F_1	0	0	0	0	+	+	0
V_0	0	0	0	0	+	+	0
V_1	0	0	0	0	+	+	0
W_L	0	x[d]	0	0	x	x	0
WW_L	0	0	x	x	0	0	0
N	x	x	x	0	x	x	x
NN[c]	0	0	0	x	0	0	0
U	+/0[e] (U_L)	+/0 (U_L)	0	0	+ (U_F)	+ (U_F)	+/0 (U_L)
A_2	0	0	0	0	+	0	0
AA_2	0	0	0	0	0	+	0
DD	0	0	0	0	0	0	x

[a]according to [8]; [b]sign "+" means that the load acts; [c]sign "0" means that the load does not act; [c]transport inclination (10%); [d]load action caused by longitudinal wind, inclination and earthquake in "x" direction (Fig. 3); [e]influence of U_L is taken into consideration (+) for $z_{UL}>0$

When considering static stability, according to [9] all of the SS loads are divided into two groups. The first group (G1) consists of permanently acting forces of constant intensity (stabilizing forces – dead weight), while the second group (G2) consists of loads not acting permanently (overturning forces).

In general, depending on load conditions, and also on the geometric configuration of the SS (Fig. 3) violation of static stability is possible in two cases: (1) the loss of static stability on the bucket wheel side (case: BWS); (2) the loss of static stability on the counterweight side (case: CWS). In the first case the load combinations which give maximum winch rope forces are representative (Table 1) while in the second case the representative load combinations are those which cause minimum winch rope forces (Table 2).

[a]according to [8]; [b]sign ''+'' means that the load acts; [c]sign ''0'' means that the load does not act; [d]normal inclination (5%); [e]earthquake (11%); [f]load action caused by longitudinal wind, inclination and earthquake in ''–x'' direction (Fig. 3)

Static stability of the SS is obtained by its own dead weight:

$$G_{SS} = \sum_i G_i,\ \text{i=BWB, M1, BWBS, CWB, M2, CWBS, SP, CW,} \tag{8}$$

thus, its COG position:

$$\chi_{SS} = \sum_i G_i \chi_i,\ \chi = x, y, z,\ \text{i=BWB, M1, BWBS, CWB, M2, CWBS, SP, CW,} \tag{9}$$

related to the coordinate system *Oxyz* (whose applicate is coinciding with the SS slewing axis, Fig. 3) must be determined precisely. Abscissas and applicates of BWB, BWBS and M1 centers of gravity are dependent on the BWB hoisting angle (Fig. 2):

$$\chi_i = \chi_{1,i}(\alpha_{BWB}) + \chi_{O1},\ \chi=x,z,\ i=BWB, M1, BWBS, \quad (10)$$

which cause dependence of the complete SS COG position on the position of the BWB.

Positions of the points of application of the total vertical and longitudinal horizontal loading of the SS, caused by forces which belong to G2, are also dependent on the BWB hoisting angle. Besides, it is important to note that: (a) the direction of vertical loading belonging to G2 is constant, thus, it does not depend on the analyzed case of static stability loss (BWS or CWS); (b) the direction of longitudinal horizontal loading belonging to G2, with the exception of cutting force U_L, depends on the analyzed case of static stability loss; (c) all of the analyzed loads (Tables 1 and 2) are acting in planes parallel to plane *Oxz* and therefore do not have components along the direction of *y* axis (Fig. 3).

By reducing all forces acting upon the SS in point *O* (Tables 1 and 2, Fig. 3) the static system of the SS loading yields to the principal vector and principal moment with coordinates:

$$X = \sum_i X_i, \quad (11)$$

$$Z = \sum_i Z_i, \quad (12)$$

$$M_x = \sum_i Z_i y_i, \quad (13)$$

$$M_y = \sum_i (X_i z_i - Z_i x_i), \quad (14)$$

$$M_z = -\sum_i X_i y_i, \quad (15)$$

where X_i and Z_i are coordinates of partial loadings, while x_i, y_i and z_i are coordinates of the mentioned partial loadings points of application.

The $\vec{k}M_z$ component of the principal moment does not act upon the slew bearing, but upon the open gear transmission of the SS slewing drive. Therefore, the slew bearing is loaded by components $\vec{i}M_x$ and $\vec{j}M_y$ of the principal moment i.e. by the moment $\vec{M} = \vec{i}M_x + \vec{j}M_y$. The position of the moment $\vec{M}$ plane of action (Fig. 4) is determined by the angle:

$$\xi = \operatorname{arctg}\frac{M_y}{M_x}. \quad (16)$$

The acting plane of moment $\vec{M}$ is perpendicular to the *Oxy* plane, and their intersecting line (line *m*) forms with *x* axis the angle:

$$\xi_m = \xi - \frac{\pi}{2}, \text{ for } \xi > 0, \quad (17a)$$

$$\xi_m = \xi + \frac{\pi}{2}, \text{ for } \xi < 0. \quad (17b)$$

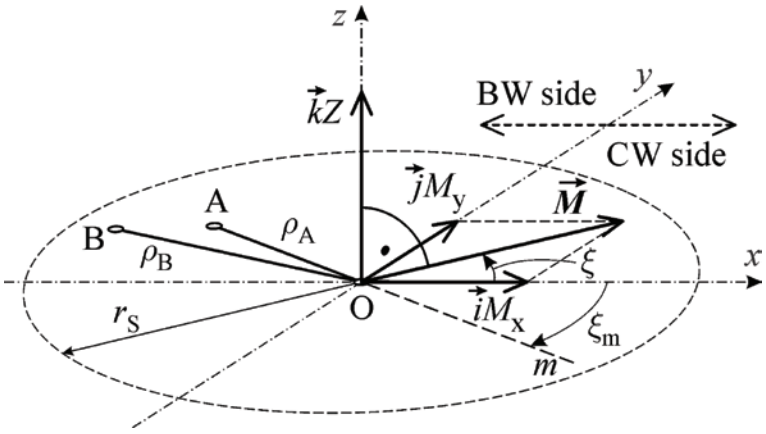

Fig. 4. The scheme for determining the distance of the total SS loading principal vector penetration point through referent plane of the RSB: Oxy-RSB referent plane; A-penetration point for the case of unfactored forces of both G1 and G2 groups; B-penetration point for the case of unfactored forces of group G1 and factored forces of group G2; $\vec{M}$ -moment acting upon RSB; $\vec{i}M_x$, $\vec{j}M_y$ -components of moment $\vec{M}$; $\vec{k}Z$ - component of the principal vector; ξ-angle between the moment $\vec{M}$ and the x axis; m-intersecting line between the moment $\vec{M}$ plane of action and the RSB referent plane; ξm-angle between line m and x axis; rS-radius of stability contour; ρA-distance of point A from the slewing axis; ρB-distance of point B from the slewing axis

The $\vec{k}Z$ component of the principal vector is perpendicular to moment $\vec{M}$ (Fig. 4), meaning that their action is equivalent to the action of force $\vec{k}Z$ with line of action passing through point *A* with coordinates:

$$x_A = -\frac{M_y}{Z}, \quad (18)$$

$$y_A = \frac{M_x}{Z}. \quad (19)$$

Point *A* belongs to the line *m* and is at the distance of:

$$\rho_A = \sqrt{x_A^2 + y_A^2} \quad (20)$$

from point *O*. Point *A*, determined in such a way, also represents the point of penetration of the total loading (unfactored forces of both G1 and G2 groups) of the SS principal vector line of action.

According to [8] contour of stability, i.e. the calculating contour of leaning in the plane of the slew bearing, is a circle with a radius of:

$$r_S = 0.95 r_{SB}, \quad (21)$$

with r_{SB} being the radius of the slew bearing rolling path.
The necessary condition of the SS static stability is:

$$\rho_{A,max} < r_S, \quad (22)$$

where $\rho_{A,max}$ is the maximum distance of point A from the SS slewing axis.

The minimum values of safety factors against overturning, prescribed by the standard [8] are dependent on the analyzed load case: for LCsH, $v_{H,min}$=1.5; for LCsHZ, $v_{HZ,min}$=1.33; for LCsHZS, $v_{HZS,min}$=1.2; for LCsHZG, $v_{HZG,min}$=1.1. When the forces belonging to G2 are factored with corresponding values of safety factors and the calculation is conducted according to expressions (11-20), coordinates of point B (point of penetration of the principal vector line of action in case of unfactored forces of group G1 and factored forces of group G2) and its distance from the SS slewing axis can be obtained. The sufficient condition of the static stability is:

$$\rho_{B,max} < r_S , \tag{23}$$

where $\rho_{B,max}$ is the maximum distance of point B from the SS slewing axis (Fig. 4).

The penetration point (C) of the overturning forces principal vector (unfactored forces of group G2) line of action through the referent plane of slew bearing, whose position is determined according to expressions (11-20), belongs to line n which intersects the stability contour in point T (Fig. 5). Tangent t on the stability contour in point T is the line of possible overturning.

Distance between points C and T is:

$$l_T = \rho_{C,max} - r_S . \tag{24}$$

The length of the line segment $\overline{ET}$ (Fig. 5) and the distance between points C_{SS} and F are determined according to expressions:

$$\overline{ET} = r_S \sin\xi_n + y_{SS} , \text{ for case BWS;} \tag{25a}$$

$$\overline{ET} = r_S \sin\xi_n - y_{SS} , \text{ for case CWS;} \tag{25b}$$

$$\overline{C_{SS}F} = x_{SS} + r_S \cos\xi_n + \overline{EF} = x_{SS} + r_S \cos\xi_n + \overline{ET}\,\mathrm{tg}\xi_n = \\ = x_{SS} + r_S \cos\xi_n + (r_S \sin\xi_n + y_{SS})\,\mathrm{tg}\xi_n , \text{ for case BWS;} \tag{26a}$$

$$\overline{C_{SS}F} = r_S \cos\xi_n - x_{SS} + \overline{EF} = r_S \cos\xi_n - x_{SS} + \overline{ET}\,\mathrm{tg}\xi_n = \\ = r_S \cos\xi_n - x_{SS} + (r_S \sin\xi_n - y_{SS})\,\mathrm{tg}\xi_n , \text{ for case CWS.} \tag{26b}$$

Finally, the distance of the SS COG from the tipping line t is calculated according to the equations:

$$l_S = \overline{C_{SS}F}\cos\xi_n = \left[x_{SS} + r_S \cos\xi_n + (r_S \sin\xi_n + y_{SS})\mathrm{tg}\xi_n\right]\cos\xi_n , \text{ for case BWS;} \tag{27a}$$

$$l_S = \overline{C_{SS}F}\cos\xi_n = \left[r_S \cos\xi_n - x_{SS} + (r_S \sin\xi_n - y_{SS})\mathrm{tg}\xi_n\right]\cos\xi_n , \text{ for case CWS.} \tag{27b}$$

The intensity of the overturning moment is calculated according to the expressions:

$$M_T = |Z_{G2}|\, l_T , \text{ for ZG2}\neq 0; \tag{28a}$$

$$M_T = \sum_L k_L L z_L , \text{ L=WL,WWL,N,NN,UL,DD, for ZG2=0,} \tag{28b}$$

where L is the intensity of corresponding longitudinal horizontal force, z_L is the applicate of its point of action, while k_L is the indicator of analyzed influence existence, according to Table 2 (if ''0'' stands in the corresponding field, k_L=0; otherwise, k_L=1).

The ratio between the moment of stability:

$$M_S = G_{SS} l_S , \tag{29}$$

and the overturning moment, expressions (28):

$$\nu = \frac{M_T}{M_S} , \tag{30}$$

presents the factor of safety against overturning, whose value must meet the criterion:

$$\nu \geq \nu_{DIN} , \tag{31}$$

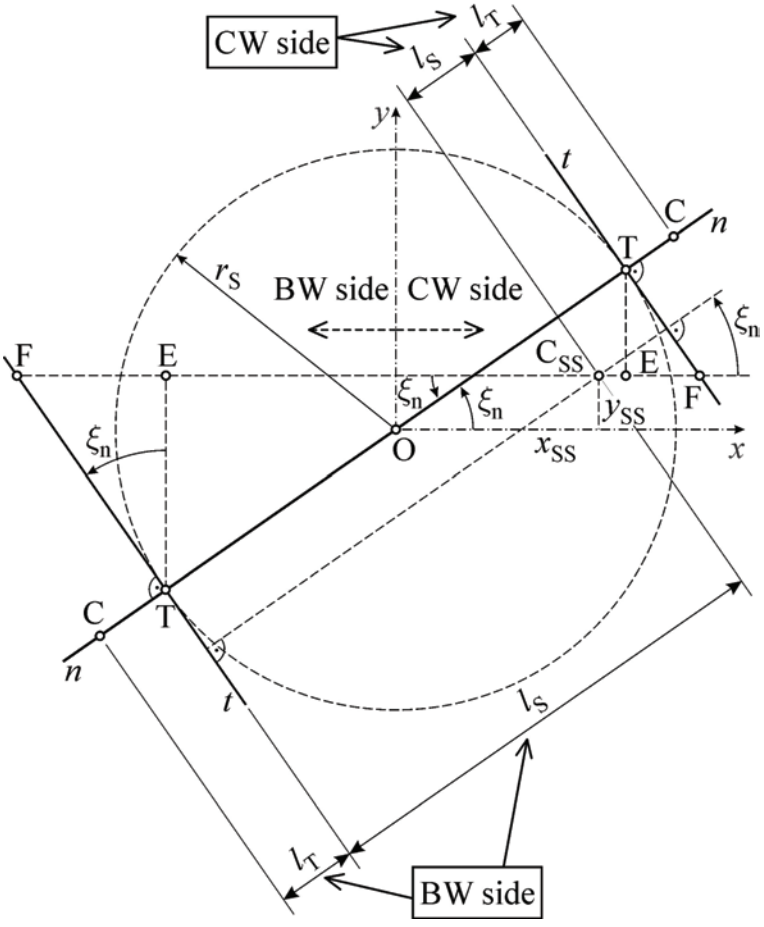

Fig. 5. The scheme for determining the distance of the SS center of gravity (CSS) and penetrating point of the overturning forces principal vector line of action (C) from the line of possible overturning: Oxy-RSB referent plane; n-intersecting line between the overturning moment plane of action and the RSB plane; rS-radius of stability contour; T-the point of intersection between the line n and the stability contour; t-line of possible overturning (tipping line); ξn-angle between intersecting line n and x axis; $\overline{OC}$ =ρC,max; lT-distance between the points C and T; lS-distance between the points CSS and T; E,F-auxiliary points for geometry calculations

Table 3. Positions[a] of points O_1 and O_{BW}

Point	Coordinates		
	x (m)	y (m)	z (m)
O_{BW}[b]	–36.288	–0.76	0.36
O_1[c]	–3.878	0	3.675

[a]Fig. 3.;[b]related to the $O_1x_1y_1z_1$ coordinate system for α_{BWB}=0; [c]related to the Oxyz coordinate system

Table 4. Weights[a] and centers of gravity positions[b] of the SS substructures (forces belonging to G1)

Notation	Weight (kN)	Coordinates		
		x (m)	y (m)	z (m)
G_{BWB}	3992.582	–26.693[c]	–0.35	0.931
G_{M1}	593.770	–4.656[c]	0	17.624
G_{CWB}	2440.483	26.296[d]	0.05	12.526
G_{M2}	778.561	3.773[d]	–0.219	22.688
G_{SP}	1782.605	0.33[d]	0	1.375
G_{CW}	2168.801	34.123[d]	0	10.075

[a]weights of BWBS, CWBS and winch ropes are added to weights of BWB, M1, M2 and CWB; [b]Fig. 3; [c]related to the $O_1x_1y_1z_1$ coordinate system for α_{BWB}=0; [d]related to the Oxyz coordinate system

Table 5. Intensities and positions[a] of points of application of forces belonging to G2

Notation	Intensity (kN)	x (m)	y (m)	z (m)
F_1	376.1	–18.1[b]	0.85	0.8
V_0	196.6	–36.288[b]	–0.76	0
V_1	37.61	–18.1[b]	0.85	0.8
VV_1	597	–35.3[b]	0.9	2.5
W_L/WW_L				
BWB	92.6	–23.433[b]	0	1.034
M1	16.7	–2.91[b]	0	14.329
CWB	90.7	20.116[c]	0	10.725
M2	20.0	3.878[c]	0	20.661
SP	19.7			
N/NN				
BWB	199.629	–26.693[b]	–0.35	0.931
M1	29.689	–4.656[b]	0	17.624
CWB	122.024	26.296[c]	0.05	12.526
M2	38.928	3.773[c]	–0.219	22.688
SP	89.13	0.33[c]	0	1.375
CW	108.401	34.123[c]	0	10.075
F1	18.805	–18.1[b]	0.85	0.8
V0	9.83	–36.288[b]	–0.76	0
V1	1.881	–18.1[b]	0.85	0.8
VV1	29.85	–35.3[b]	0.9	2.5
U_F/UU_F	505.1/658.802	–42.413[b]	–0.12	0.36
U_L/UU_L	505.1/658.802	–36.288[b]	–0.12	–5.765
DD				
BWB	439.184	–26.693[b]	–0.35	0.931
M1	65.315	–4.656[b]	0	17.624
CWB	268.453	26.296[c]	0.05	12.526
M2	85.642	3.773[c]	–0.219	22.688
SP	196.087	0.33[c]	0	1.375
CW	268.453	34.123[c]	0	10.075
F_1	41.371	–18.1[b]	0.85	0.8
V_0	21.626	–36.288[b]	–0.76	0
V_1	4.137	–18.1[b]	0.85	0.8
VV_1	65.67	–35.3[b]	0.9	2.5

[a]Fig. 3; [b]related to the $O_1x_1y_1z_1$ coordinate system for α_{BWB}=0; [c]related to the Oxyz coordinate system

with v_{DIN} being the value of safety factor prescribed by code [4] for the considered load case.

Procedures for the static stability proof 'a priori' and 'a posteriori' are the same, but for conducting an 'a posteriori' procedure it is first of all necessary to determine the 'corrective mass' and its COG on the basis of weighing results, according to the procedure presented in [5].

3. Numerical example

Calculations and comparison of the obtained results were conducted using the in-house developed software STEX. This software enables the determination of all the variables needed for static stability analysis on the whole domain of the BWB hoisting angle ($-19.52° \leq \alpha_{BWB} \leq 14.1°$). Input data (Tables 3-5) are taken from the final stability calculation (''a priori'') provided by the manufacturer of the BWE 1600 (variant V2 in [5]). The positions of acting points of all the forces acting upon SuS1, related to the coordinate system *Oxyz*,

Table 6. Setting values of the winch rope forces: V2

Rope force	S_A (kN)	S_{AA} (kN)	S_Z (kN)	S_{ZZ} (kN)
Setting value	197.4	182.7	342.5	358.3

Table 7. Position of the 'corrective mass' COG related to the Oxyz coordinate system

BWB position	x_C (m)	y_C (m)
L: $\alpha_{BWB}=-12.9°$	−22.39	0.047
H	−22.824	0.311
Hi: $\alpha_{BWB}=14.1°$	−21.199	0.507

Table 8. 'Corrective mass' COG position related to the moving coordinate system $O_1\xi\eta\zeta$

ξ_C (m)	η_C (m)	ζ_C (m)
18.946	0.288	3.29

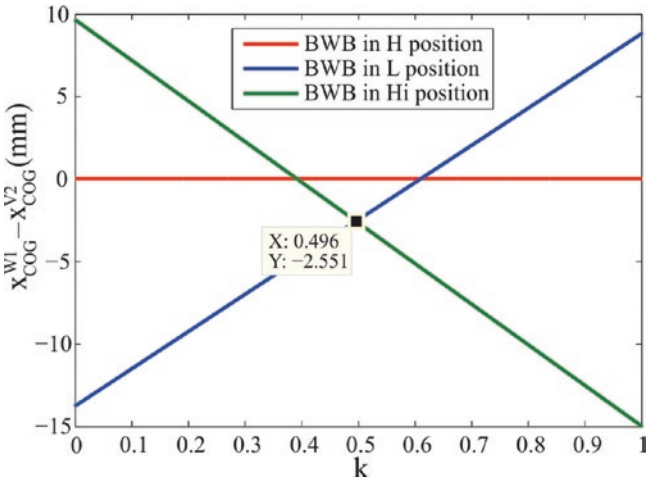

Fig. 9. Deviation of the 'corrective mass' COG abscissa

are determined by the appropriate transformations of coordinates related to the coordinate system $Ox_1y_1z_1$ (Fig. 3).

According to expressions (1)–(4), the maximum and minimum intensities of winch rope forces for LC HZ3.1 ($S_{HZ3.1,max}$=317.1 kN, $S_{HZ3.1,min}$=210.0 kN, Fig. 6), are used as the basis for determining the setting values of the rope forces (Table 6). They determine the intensities of ground reactions when partial leaning of the BW appears, as well as overload forces, equations (6) and (7), Figs. 7 and 8.

Using the procedure and data presented in [5, Subsection 6, expressions (1)–(6)] the 'corrective mass' is determined as follows:

$$\Delta m_S^{V2} = m_{S,W1,A} - m_{S,CW1}^{V2} = 1172.263 - 1154.387 = 17.876 \text{ t},$$

as well as its COG in measuring positions of the BWB:

$$\chi_{C,i} = \frac{G_{S,i}^{W1} x_{COG,i}^{W1} - m_{S,CW1}^{V2} g x_{COG,i}^{V2}}{\Delta m_S^{V2} g}, \ \chi = x, y,$$

where i=L, H, Hi presents the indicator of the BWB measuring posi-

Table 9. BPSS: V2 vs. V5 vs. W1[a]

Variant	Total mass	CW mass	Total mass without CW	x_{COG} (mm)		
				L	H	Hi
	(t)			α_{BWB} (°)		
				−12.9	0	14.1
V2	1154.387	177.017	977.370	−51	−15	581
V5	1172.263	177.017	995.246	−396	−356	252
W1	1172.263	177.017	995.246	−398	−356	249

[a] *Weighing 1 [5]*

Table 10. Distances of penetration points A and B from the slewing axis (BWS)

Load case	$\rho_{A,max}$ (m)		$\rho_{B,max}$ (m)	
	V2	V5	V2	V5
H1.1	2.44	2.714	4.027	4.271
HZ3.1	2.603	2.874	3.717	3.967
HZ3.2	0.564	0.878	1.134	1.442
HZS4.4	4.236	4.475	5.162	5.384
HZS4.8	4.495	4.723	5.504	5.714
HZG5.3	5.092	5.310	5.643	5.851
HZG5.4	3.334	3.604	3.753	4.017

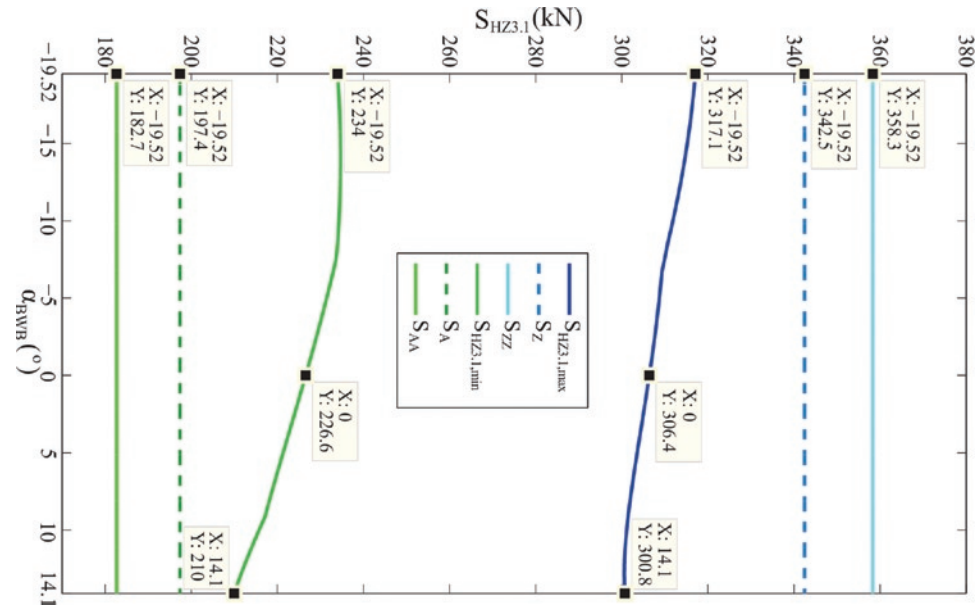

Fig. 6. Rope force in LC HZ3.1 and setting values of the winch rope forces: V2

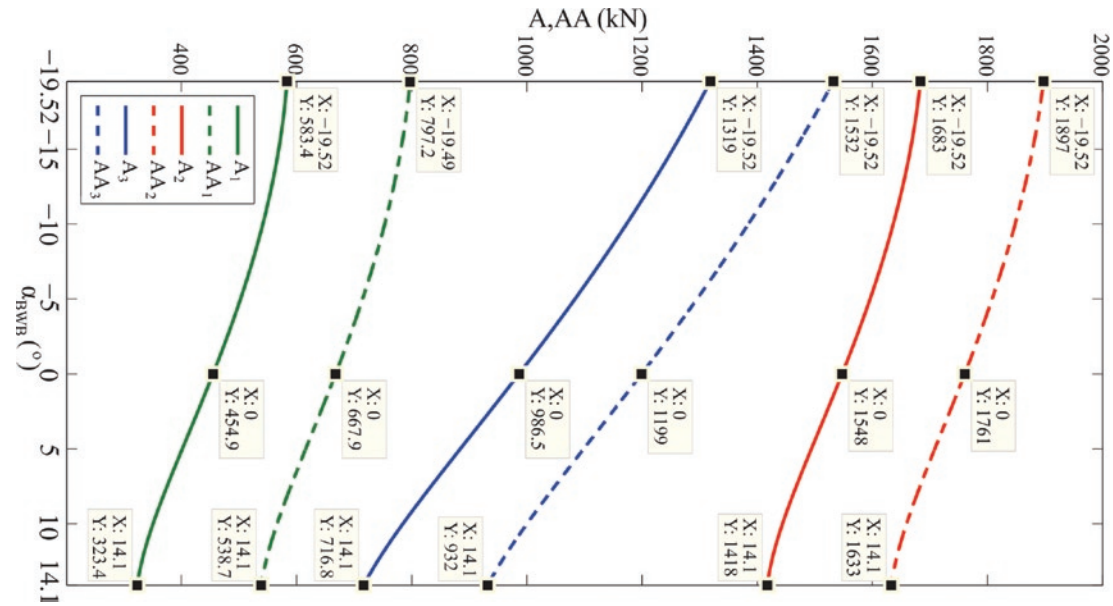

Fig. 7. Ground reactions due to partial leaning of the BW: V2 (for LC 1, LC 2 and LC 3)

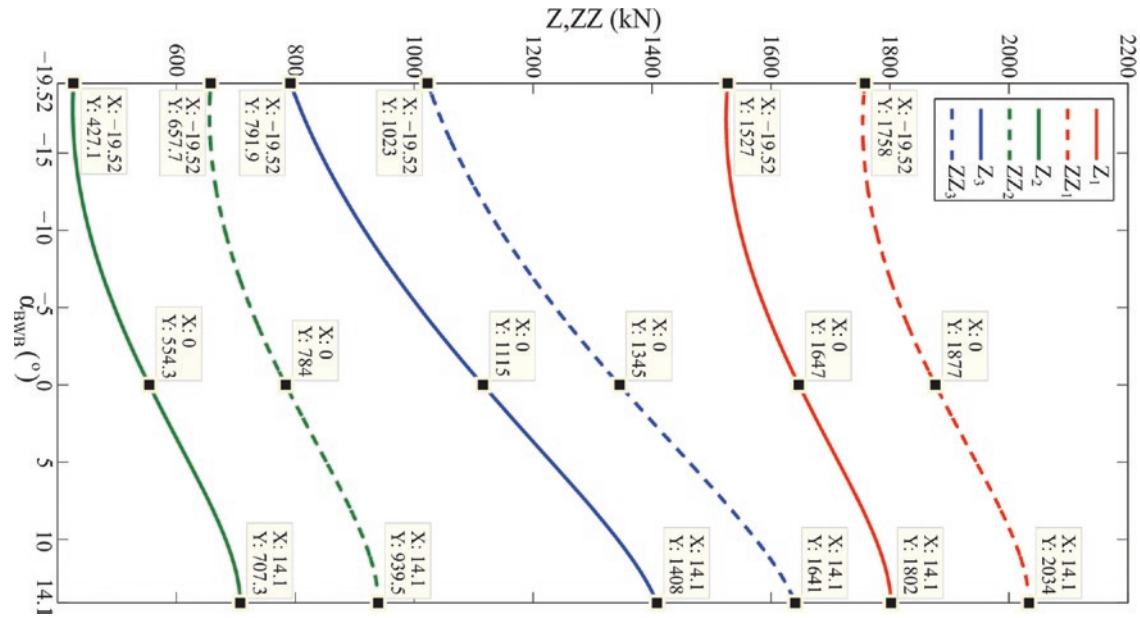

Fig. 8. Overload forces: V2 (for LC 1, LC 2 and LC 3)

Table 11. Distances of penetration points A and B from the slewing axis (CWS)

Load case	$\rho_{A,max}$ (m)		$\rho_{B,max}$ (m)	
	V2	V5	V2	V5
H1.1	2.657	2.317	3.077	2.735
HZ3.1	2.890	2.585	3.245	2.899
HZ3.2	3.124	2.819	3.556	3.206
HZS4.1	3.676	3.379	4.048	3.699
HZS4.7	4.149	3.739	4.739	4.316
HZG5.2	4.974	4.543	5.363	4.923
HZG5.4	3.870	3.531	4.075	3.736

Table 12. Minimum safety factors and corresponding BWB hoisting angles and angles of possible overturning planes (BWS)

Load case	ν_{min}		α_{BWB} (°)		ξ_n (°)	
	V2	V5	V2	V5	V2	V5
H1.1	1.906	1.827	−1.1	−1.34	−0.18	−0.18
HZ3.1	1.806	1.732	0.03	−0.26	−0.17	−0.17
HZ3.2	3.628	3.489	12.9	12.05	0.28	0.28
HZS4.4	1.214	1.165	−1.66	−1.9	−0.55	−0.55
HZS4.8	1.144	1.100	7.25	6.83	0.98	0.97
HZG5.3	1.024	0.985	6.42	5.97	0.99	0.99
HZG5.4	1.463	1.401	5.0	4.6	−0.14	−0.14

Table 13. Minimum safety factors and corresponding BWB hoisting angles and angles of possible overturning planes (CWS)

Load case	ν_{min}		α_{BWB} (°)		ξ_n (°)	
	V2	V5	V2	V5	V2	V5
H1.1	4.056	4.476	14.1	14.1	0	0
HZ3.1	3.174	3.51	14.1	14.1	0	0
HZ3.2	2.606	2.887	14.1	14.1	0	0
HZS4.1	1.834	2.025	14.1	14.1	0	0
HZS4.7	1.363	1.508	−19.52	−19.52	0.05	0.05
HZG5.2	1.066	1.179	−19.52	−19.52	0.04	0.04
HZG5.4	1.66	1.827	14.1	14.1	0	0

Table 14. BPSS. V5 vs. W2 (α_{BWB}=−11.4°, m_{CW}=231.977 t)

Variant	CW mass (t)	Total mass (t)	Coordinates of the COG (mm)	
			x_{COG}	y_{COG}
V5	231.977	1227.223	1130	−116
W2	231.977	1233.772	1087	−130

tion (Table 7).

The abscissa and the applicate of the 'corrective mass' COG related to the moving coordinate system $O_1\xi\eta\zeta$ are determined according to the expressions given in [3, equations (7)–(9)] with the adopted value of the corrective factor k=0.496, while the ordinate is determined as the average of ordinates obtained for the analyzed measuring positions (Table 8).

When transforming V2 to V5 in the paper [5] during the process of determination of the applicate of the 'corrective mass' COG, the value of the corrective factor k=0.5 was adopted and used. In the analysis to follow, a more precise value of the mentioned factor of k=0.496 was used (Fig. 9, Table 9).

The radius of the slew bearing is 5.5 m, so, according to the expression (21), the radius of the stability contour is

$$r_S = 0.95 r_{SB} = 0.95 \times 5.5 = 5.225 \text{ m}.$$

Positions of the penetration points A and B, as well as the values of the factor of safety against overturning, calculated 'a priori' (V2) and 'a posteriori' (V5), are presented in Tables 10−13. Dependence of the factors of safety on the BWB hoisting angle for critical load cases is shown in Figs. 10−13.

Control weighing (W2) was conducted after the correction of the CW mass, with CW of 231.977 t [5, Subsection 5], Table 14.

The weight of the 'corrective mass' causes changes of winch rope force intensity making it necessary to correct the setting values ac-

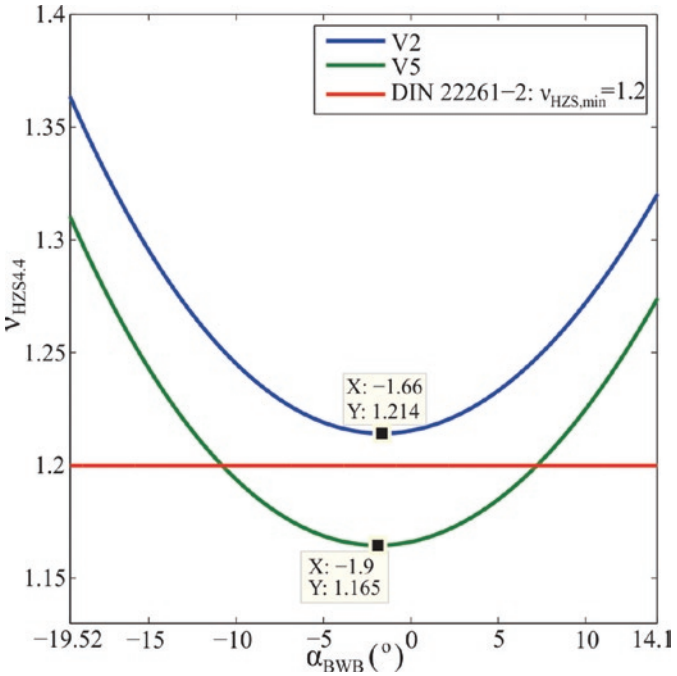

Fig. 10. Safety factor in the LC HZS4.4 (BWS)

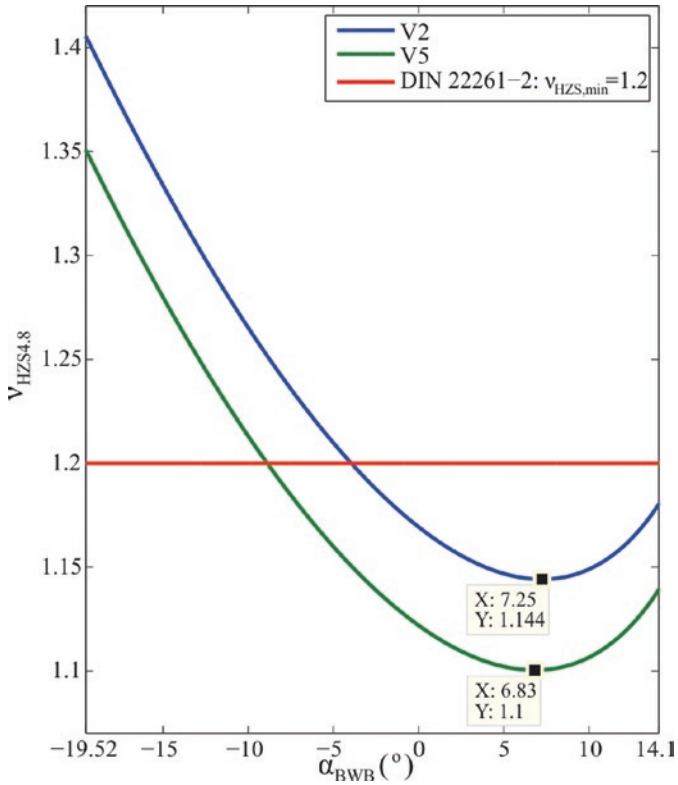

Fig. 11. Safety factor in the LC HZS4.8 (BWS)

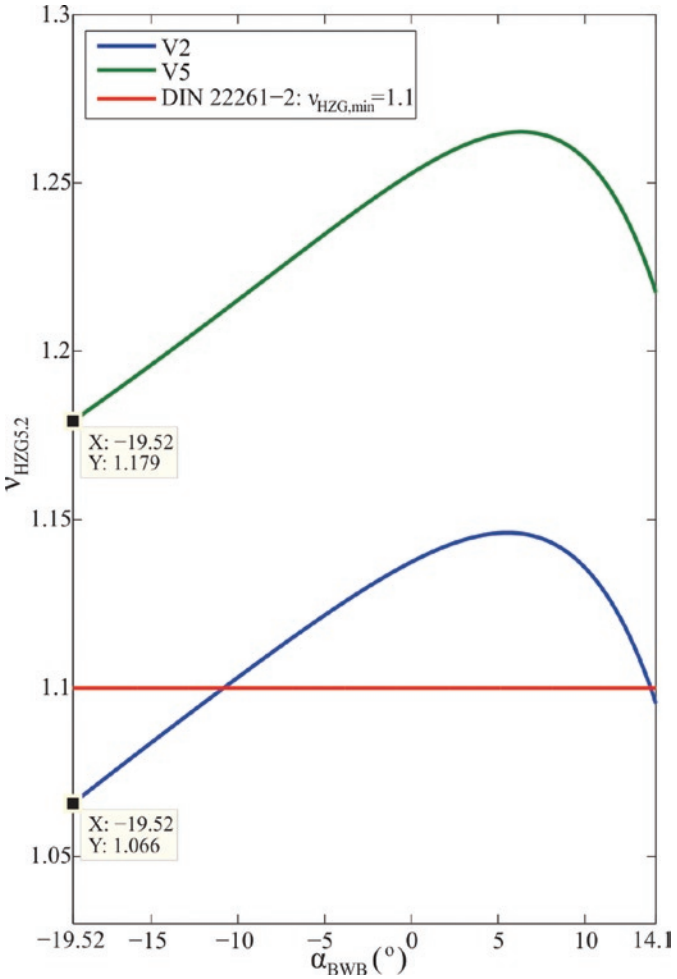

Fig. 12. Safety factor in the LC HZG5.2 (CWS)

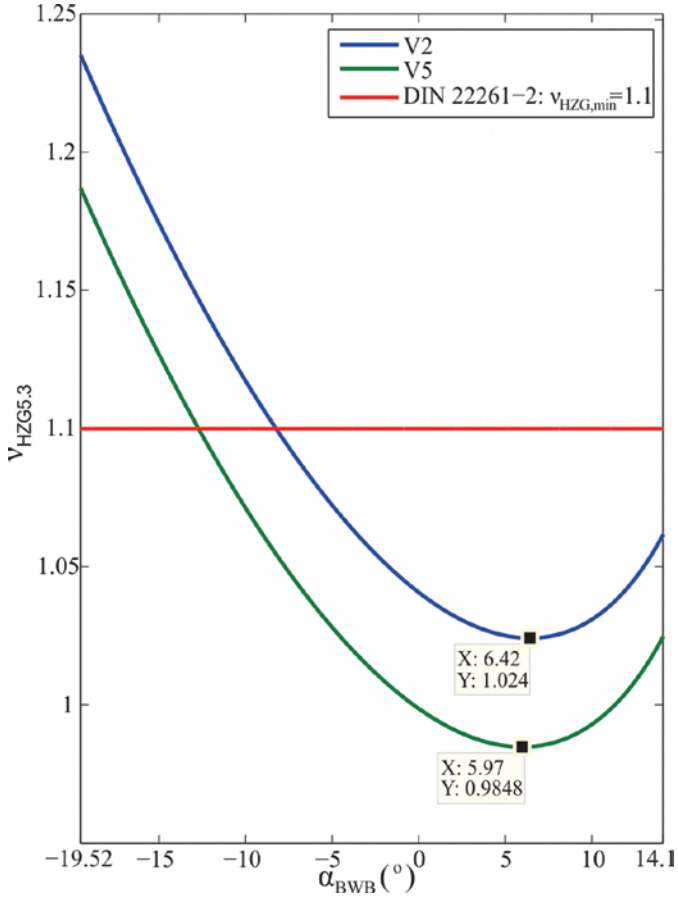

Fig. 13. Safety factor in the LC HZG5.3 (BWS)

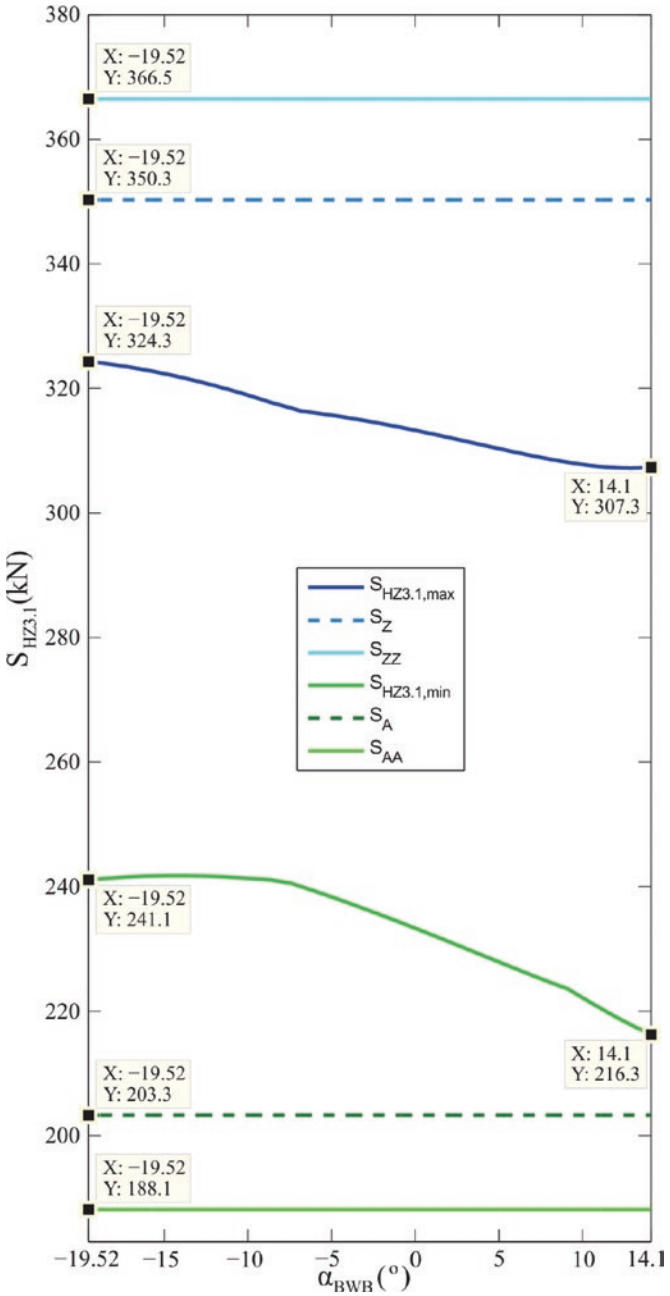

Fig. 14. Setting values of winch rope forces: V5

cording to equations (1)−(4), (Fig. 14, Table 15). The modification of the CW mass in relation to the designed one, caused changes of positions of the points *A* and *B* (Tables 16 and 17) as well as changes of safety factor values (Tables 18 and 19).

4. Discussion

The SS for V2 fulfills the necessary condition of static stability. For all the referent load cases, the distance of penetration point *A* from the slewing axis (Tables 10 and 11) fulfills the condition defined by expression (22). The maximum distance value of $\rho_{A,max}$=5.092 m which is obtained for the LC HZG5.3 (BWS) is lower than the value of the stability contour radius defined by the expression (21), r_S=5.225 m. However, in LCs HZS4.8, HZG5.2 and HZG5.3 the distances of point *B* from the slewing axis are greater than the radius of the stability contour, which means that in the described load cases the condition defined by the expression (23) is not fulfilled. Consequently, in the above-mentioned LCs, safety factors are lower than those prescribed by standard [8] (Tables 12 and 13, Figs. 10−13).

The 'corrective mass' and its COG position were determined on the basis of measurement 1 conducted after the first erection (Table 9) using the procedure presented in [5, Subsection 2]. Variant V2 was transformed into variant V5 by implementing the influence of the corrective mass. By adopting the corrective factor value of k=0.496, the absolute values of COG abscissa deviations, as opposed to those determined by measurement 1, become lower than 3 mm (Fig. 9, Table 9). Variant V5, formed in that manner, presents the actual image of the SS, as opposed to the V2, which is the designed (desired) image of the SS.

The excessive mass ('corrective mass') on the side of the BW causes deviation of the penetration points *A* and *B* distances from the slewing axis (Tables 20 and 21). An increase of referent distances (Table 20) worsens the stability conditions on the BW side, leading to lower values of safety factors (Table 12) as well as widening of the BWB hoisting angle range within which the values of safety factors are lower than allowed (Figs. 10 and 13). Apart from the already mentioned LCs HZ4.8 and HZG5.3, the value of safety factor for V5 is also lower than the minimum value prescribed by standard [8] in the LC HZS4.4 (Fig. 10). On the other hand, in the CWS case, the decrease of referent distances improves the stability conditions, thus leading to greater safety factor values (Table 13). As opposed to V2, the SS in V5 also meets the static stability criterion in LC HZG5.2 (Fig. 12).

$$\Delta x_{COG} = x_{COG}^{W1} - x_{COG}^{V2}$$

Table 15. Setting values of winch rope forces: V5

Rope force	S_A (kN)	S_{AA} (kN)	S_Z (kN)	S_{ZZ} (kN)
Setting value	203.3	188.1	350.3	366.5

Table 16. Distances of penetration points A and B from the slewing axis: V5, m_{CW}=231.977 t (BWS)

Load case	$\rho_{A,max}$ (m)	$\rho_{B,max}$ (m)
H1.1	2.416	3.975
HZ3.1	2.576	3.669
HZ3.2	0.58	1.139
HZS4.4	4.177	5.087
HZS4.8	4.715	5.746
HZG5.3	5.305	5.866
HZG5.4	3.309	3.722

Table 17. Distances of penetration points A and B from the slewing axis: V5, m_{CW}=231.977 t (CWS)

Load case	$\rho_{O,max}$ (m)	$\rho_{O,max}^{G2,fac}$ (m)
H1.1	2.606	3.023
HZ3.1	2.876	3.184
HZ3.2	3.107	3.488
HZS4.1	3.667	3.982
HZS4.7	3.715	4.218
HZG5.2	4.529	4.872
HZG5.4	3.819	4.023

Table 18. Minimum safety factors and corresponding BWB hoisting angles and angles of possible overturning planes: V5, m_{CW}=231.977 t (BWS)

Load case	ν_{min}	α_{BWB} (°)	ξ_n (°)
H1.1	1.931	−1.12	−0.18
HZ3.1	1.83	0	−0.17
HZ3.2	3.668	12.78	0.28
HZS4.4	1.232	−1.7	−0.55
HZS4.8	1.098	6.75	0.98
HZG5.3	0.986	5.93	0.99
HZG5.4	1.476	5.04	−0.14

Table 19. Minimum safety factors and corresponding BWB hoisting angles and angles of possible overturning planes: V5, m_{CW}=231.977 t (CWS)

Load Case	ν_{min}	α_{BWB} (°)	ξ_n (°)
H1.1	4.142	14.1	0
HZ3.1	3.252	14.1	0
HZ3.2	2.677	14.1	0
HZS4.1	1.875	14.1	0
HZS4.7	1.591	−19.52	2.87
HZG5.2	1.202	−19.52	2.46
HZG5.4	1.688	14.1	0

Table 20. Differences of the penetration points A and B distances from the slewing axis (BWS)

Load case	$\rho_{A,max}^{V5} - \rho_{A,max}^{V2}$ (m)	$\rho_{B,max}^{V5} - \rho_{B,max}^{V2}$ (m)
H1.1	0.27	0.244
HZ3.1	0.271	0.25
HZ3.2	0.314	0.308
HZS4.4	0.239	0.222
HZS4.8	0.228	0.21
HZG5.3	0.218	0.208
HZG5.4	0.27	0.264

Mass distribution of the actual SS is less favorable than for the designed one, which causes shifting of the SS center of gravity towards the BW (Tables 9 and 22).

The excavator designer solved the problem of unfavorable COG shifting towards the BW by enlarging the CW mass. Based on the results of measurement 1, the mid value of the excessive moment was calculated in relation to the designed values (V2) and then divided by the distance of the CW COG from the slewing axis. That way, the weight which has to be added to the designed weight of the CW was calculated.This is the reason why the mass of the CW during the measurement 2 was 231.977 t, as opposed to the design one (V2) which was 221 t (Table 14). The difference between the SS mass determined by measurement 2 and the one obtained by V5 (6.549 t, Table 14) is predominantly the consequence of the appearance of foreign bodies and a little bit of snow [5]. Having in mind the conditions in which measurement 2 was conducted, the calculated coordinates of COG for V5 are in good correlation to those obtained by measurement 2 (Table 14).

Greater weight on the BW side, as opposed to the designed one, led to the increase of winch rope force intensity (Figs. 6 and 14) and

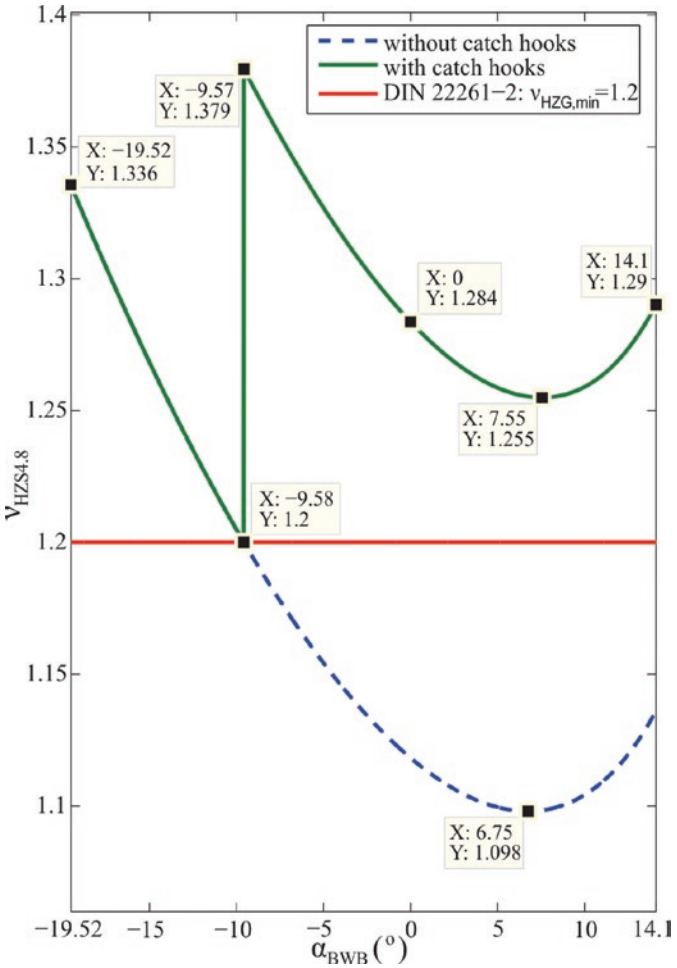

Fig. 15. Safety factor in LC HZS4.8 (BWS): V5 (m_{CW}=231.977 t)

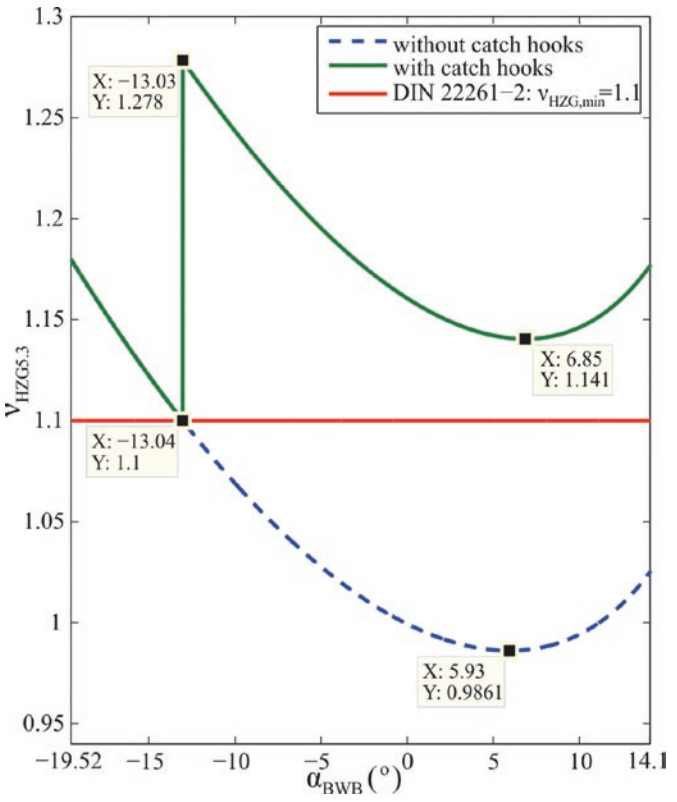

Fig. 16. Safety factor in LC HZG5.3 (BWS): V5 (m_{CW}=231.977 t)

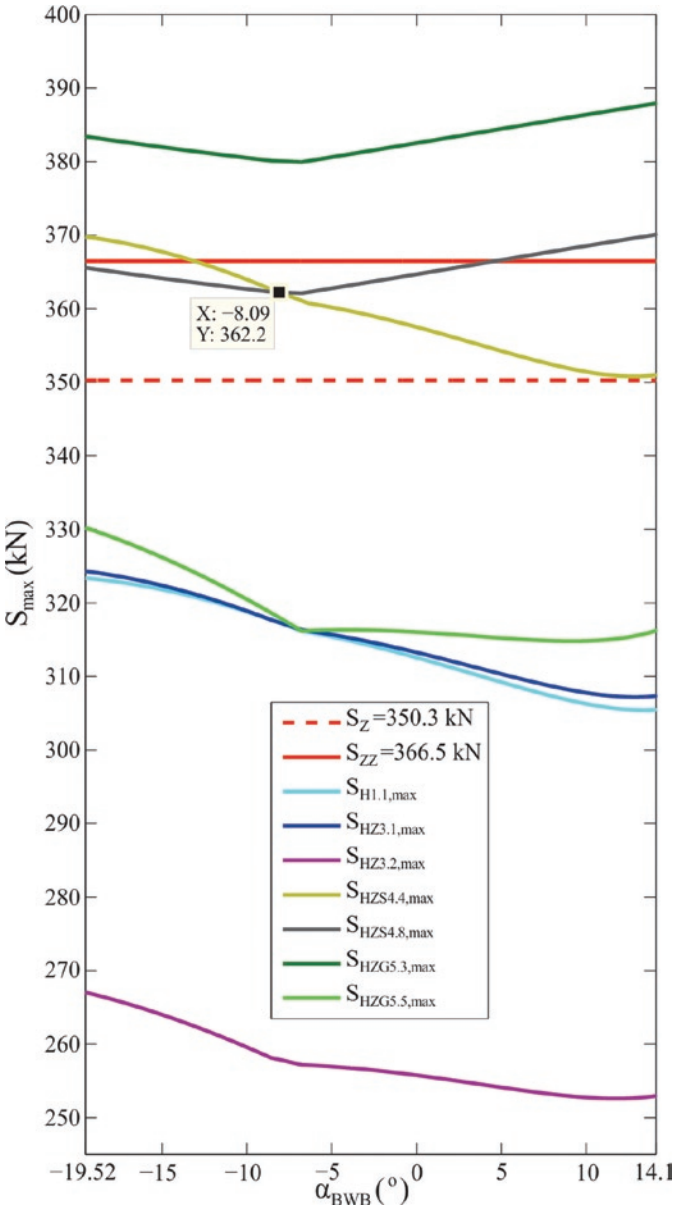

Fig. 17. Maximum winch rope forces: V5

accordingly, to the increase of setting values (Tables 6 and 15). The setting values of minimum forces are higher for ≈3.0%, while setting values of maximum winch rope forces are ≈2.3% higher.

With corrected CW mass (231.977 t) the SS fulfills the necessary condition of static stability, expression (21), as well as the sufficient one, expression (23), on the CW side (Table 17). This is confirmed by the obtained safety factor values for all the analyzed load cases (Table 19) which are higher than the minimum ones prescribed by the code [8].

When it comes to the static stability on the BW side, it can be concluded that, for all the load cases except LC HZG5.3 (Table 16) the necessary static stability condition is fulfilled. Apart from the above-mentioned load case, the sufficient static stability condition is also not fulfilled in LC HZS4.8 (Tables 16 and 18). The eventual loss of static stability in the mentioned critical load cases is prevented by activation of catch hooks (Figs. 15 and 16).

It is important to note that the SS in LC HZS4.4 fulfills the prescribed static stability condition [8], although the intensity of the maximum winch rope force is higher than that obtained for LC HZS4.8 on the BWB hoisting angle interval of $-19.52° \leq \alpha_{BWB} \leq -8.09°$ (Fig. 17).

Table 21. Differences of the penetration points A and B distances from the slewing axis (CWS)

Load case	$\rho_{A,max}^{V5} - \rho_{A,max}^{V2}$ (m)	$\rho_{B,max}^{V5} - \rho_{B,max}^{V2}$ (m)
H1.1	−0.34	−0.342
HZ3.1	−0.305	−0.346
HZ3.2	−0.305	−0.35
HZS4.1	−0.297	−0.349
HZS4.7	−0.41	−0.423
HZG5.2	−0.431	−0.44
HZG5.4	−0.339	−0.339

Table 22. Difference between the 'measured' and the projected abscissas of the SS center of gravity

Difference between GOG abscissas	BWB measuring position		
	L: α_{BWB}=−12.9°	H	Hi: α_{BWB}=14.1°
(mm)	−347	−341	−332

Table 23. Minimum safety factors and the belonging BWB hoisting angles: V5 (y_i=0), m_{CW}=231.977 t

Load case	BWS		CWS	
	ν_{min}	α_{BWB} (°)	ν_{min}	α_{BWB} (°)
H1b	1.931	−1.12	4.142	14.1
HZ2	1.83	0	3.252	14.1
HZ3	3.668	12.78	2.677	14.1
HZS4			1.875	14.1
HZS5	1.231	−1.7		
HZS8			1.59	−19.52
HZS9	1.099	6.75		
HZG13			1.202	−19.52
HZG14	0.986	5.93		
HZG15	1.476	5.04	1.688	14.1

This is explained by the influence of the SS geometric configuration, primarily by the mutual position of axis O_1y_1 and tipping line t (Figs. 3 and 5), which is decisive for the calculation of intensities of winch rope forces and moments of overturning and stability, and also by the positions of loads in the discussed load cases.

Having in mind the fact that the angles ξ_n defining the plane of overturning are relatively small (Tables 12, 13, 18 and 19), in the analysis that follows, the presented results, (Table 23), were obtained by introducing the presumption that the eccentricities of all forces acting upon the SS, in the relation to the plane *Oxz* (Tables 4 and 5) are equal to zero (i.e. y_i=0).

Based on the comparative analysis of results (Tables 18, 19 and 23), it can be concluded that, for the adopted level of accuracy, the calculation model with y_i=0 gives equal values of safety factors and values of corresponding BWB hoisting angles, as the one including the influence of loads eccentricities in relation to the *Oxz* plane.

In engineering practice, it is common to conduct the static stability calculation only for characteristic BWB positions: L (α_{BWB}=−19.52°), H (α_{BWB}=0) and Hi (α_{BWB}=14.1°). Calculation results (Tables 13, 19 and 23) show that this kind of approach might be used when dealing with the stability on the side of the CW. On the other hand, when the stability on the BW side is in question, it can be observed that there are some load cases within the minimal safety factor values obtained for BWB positions which are neither close to the H nor to the Hi position (Tables 12, 18 and 23). For example, in LC HZS4.8, the minimal value of safety factor of ν_{min}=1.255 (with catch hooks) is obtained for the BWB hoisting angle of α_{BWB}=7.55° (Fig. 15). The mentioned value is ≈2.3% and ≈2.8% lower than those obtained for positions H and Hi, respectively.

5. Proposal of the superstructure static stability proof procedure 'a posteriori'

According to the literature which was available to the authors, the answer to the question „what to do after the superstructure weighing" is given only in [9, page 233]: „If the weighing results differ by more than a certain amount, in general 5% of the theoretical values calculated for stability, the calculation must be checked and the weighing procedure repeated. The ballast must then be adjusted according to the weighing results so that the position of the COG in the plane of the jacking points corresponds to the desired theoretical values.". Therefore, the answer is of a general character. Having in mind the extreme importance of the static stability problem, considering the presented procedures and obtained investigation results, the authors suggest the implementation of the static stability calculation procedure 'a posteriori'. Its fundamental phases are:

1. Harmonization of the calculation model with all the changes made during the development of the project and the realization

of the first erection procedure, i.e. forming of the calculation model 'a priori';
2. Conducting the first weighing immediately after the completion of the first erection procedure;
3. Calculation of weight and COG position of 'a priori' model in measuring positions of the BWB;
4. Calculation of the 'corrective mass' and its position based on the results obtained by the first measurement (weighing);
5. Forming of the 'a posteriori' model, taking into account the influence of the 'corrective mass';
6. Validation of the calculation 'a posteriori' model using the results of the first measurement;
7. Determination of the needed correction of the CW mass and setting values of winch rope forces based on the static stability calculation conducted on the 'a posteriori' model;
8. Second (control) measurement with the corrected mass of the CW;
9. Calculation of weight and COG position of the 'a posteriori' model for positions of the BWB during the second measurement;
10. Final validation of the 'a posteriori' model based on the results of the second measurement;
11. Final calculation of minimal values of factor of safety against overturning on the complete domain of the BWB hoisting angle, using the 'a posteriori' model.

6. Conclusion

The complexity of the slewing superstructure balancing problem, hence the determination of the CW mass, is the consequence of: (a) the changeability of the geometric configuration; (b) the complexity of working conditions and (c) multiple limitations of the possible set of solutions. Namely, the mass of the CW has to be determined in such a manner to fulfill the prescribed criteria of static stability in all working conditions and for all geometric configurations. Furthermore, in load cases matching the normal excavator operating conditions (LCs H1.1b), the penetration point of the total superstructure loading principal vector line, through the referent plane of the slew bearing, must not be more than one quarter of its diameter from the slewing axis. That would guarantee a reliable and long-term operation of the slew bearing. Finally, from the upper side, the mass of the CW is limited by the CWB structure carrying capacity.

Keeping in mind the fact that the existing referent literature does not specify the procedure of static stability proof, this paper is the first to present it in detail. The transformation of the calculation model 'a priori' (designed image of the superstructure) to the calculation model 'a posteriori' (actual image of the superstructure) was conducted on the basis of weighing results. Calculation of all the parameters that determine the BWE superstructure static stability, for both calculation models, was conducted using the original software, developed on the basis of the above-mentioned procedure. Based on the presented calculation results, the following conclusions are derived:

- with the designed mass of the CW, the 'a priori' model fulfills the necessary condition of the static stability in all analyzed LCs, which was not the case with the 'a posteriori' model;
- with the designed mass of the CW, both models do not meet the sufficient criterion of the static stability in three LCs, two of which are the same;
- with the corrected mass of the CW, the 'a posteriori' model does not fulfill the necessary condition of the static stability in one LC, and sufficient criterion in two LCs;
- with the corrected mass of the CW, the 'a posteriori' model, which is of a spatial nature, may be reduced to the planar model of high results accuracy.

A particular contribution, achieved on the basis of the presented investigation results and perennial experience, is represented in the classification of the SS models into two fundamental groups which were named the 'a priori' and the 'a posteriori' models, as well as the fact that the basic stages of the 'a posteriori' model forming are presented in a paper. The 'a posteriori' models enable a reliable calculation of the SS static stability and may be used not only for static stability proof of the machine as a whole, but also for loads analysis of substructures and elements of BWEs and related surface mining machines – spreaders. Moreover, previously-mentioned models are of extreme importance for a successful and reliable exploitation of the machine since they present the basis for:

- adjustment and control of limiting winch rope forces values;
- periodic control of mass and center of gravity position;
- eventual reconstruction, which would be conducted in order to realize better customization of the machine versus operating conditions;

which is of extreme importance having in mind the fact that bucket wheel excavators and spreaders are machines intended (designed) for perennial exploitation.

Acknowledgement

This work is a contribution to the Ministry of Education, Science and Technological Development of Serbia funded project TR 35006.

References

1. Augustynowicz J, Dudek K, Figiel A, Nowak J, Kluczkiewicz W. Doświadczalne wyznaczanie położenia środka ciężkości obrotowego nadwozia koparek kołowych. Górnictwo Odkrywkowe 2011; 52(3-4): 92-95.
2. Bošnjak S, Zrnić N. Dynamics, failures, redesigning and environmentally friendly technologies in surface mining systems. Archives of Civil and Mechanical Engineering 2012; 12(3): 348-359, https://doi.org/10.1016/j.acme.2012.06.009.
3. Bošnjak S, Petković Z, Dunjić M, Gnjatović N, Đorđević M. Redesign of the vital subsystems as a way of extending the bucket wheel excavators life. Technics Technologies Education Management 2012; 7(4): 1620-1629.
4. Bošnjak S, Oguamanam D, Zrnić N. The influence of constructive parameters on response of bucket wheel excavator superstructure in the out-of-resonance region. Archives of Civil and Mechanical Engineering 2015; 15(4): 977-985, https://doi.org/10.1016/j.acme.2015.03.009.
5. Bošnjak S, Gnjatović N, Savićević S, Pantelić M, Milenović I. Basic parameters of the static stability, loads and strength of the vital parts of a bucket wheel excavator's slewing superstructure. Journal of Zhejiang University - SCIENCE A (Applied Physics & Engineering) 2016; 17(5): 353-365, https://doi.org/10.1631/jzus.A1500037.
6. Brkić A Đ, Maneski T, Ignjatović D, Jovančić P, Spasojević Brkić V K. Diagnostics of bucket wheel excavator discharge boom dynamic performance and its reconstruction. Eksploatacja i Niezawodnosc - Maintenance and Reliability 2014; 16 (2): 188-197.
7. Bugaric U, Tanasijevic M, Polovina D, Ignjatovic D, Jovancic P. Lost production costs of the overburden excavation system caused by rubber belt failure. Eksploatacja i Niezawodnosc - Maintenance and Reliability 2012; 14 (4): 333-341.
8. DIN 22261-2. Bagger, Absetzer und Zusatsgeräte in Braunkohlentagebauen. Teil 2: Berechnungsgrundlagen. Deutsches Institut für Normung;

2006.
9. Durst W, Vogt W. Bucket Wheel Excavator, Clausthal-Zellerfeld: Trans Tech Publications, 1988.
10. Kowalczyk M, Czmochowski J, Rusiński E. Construction of diagnostic models of the states of developing fault for working parts of the multi-bucket excavator. Eksploatacja i Niezawodnosc- Maintenance and Reliability 2009; 42(2): 17-24
11. Maslak P, Przybylek G, Smolnicki T. Comparison of selected methods for the determination of the center of gravity in surface mining machines. Materials Today: Proceedings 2017: 4(5, Part 1): 5877- 5882, https://doi.org/10.1016/j.matpr.2017.06.062.
12. Nan N, Kovacs I, Popescu F. Balance control by weighting and tensiometric measurements of bucket wheel excavators. WSEAS Transactions on Systems and Control 2008; 3(11): 927-938.
13. Pietrusiak D. Evaluation of large-scale load-carrying structures of machines with the application of the dynamic effects factor. Eksploatacja i Niezawodnosc - Maintenance and Reliability 2017; 19 (4): 542-551, https://doi.org/10.17531/ein.2017.4.7.
14. Pietrusiak D, Smolnicki T, Stańco M. The influence of superstructure vibrations on operational loads in the undercarriage of bulk material handling machine. Archives of Civil and Mechanical Engineering 2017; 17(4): 855-862, https://doi.org/10.1016/j.acme.2017.03.001.
15. Rusiński E, Czmochowski J, Moczko P, Pietrusiak D. Surface Mining Machines - Problems of Maintenance and Modernization, Cham: Springer International Publishing AG, 2017, https://doi.org/10.1007/978-3-319-47792-3.
16. Smolnicki T, Stańco M, Pietrusiak, D. Distribution of loads in the large size bearing - problems of identification. Tehnički Vjesnik - Technical Gazette 2013: 20(5): 831-836.
17. Smolnicki T, Pękalski G, Jakubik J, Harnatkiewicz P. Investigation into wear mechanisms of the bearing raceway used in bucket wheel excavators. Archives of Civil and Mechanical Engineering 2017: 17(1):1-8, https://doi.org/10.1016/j.acme.2016.07.008.

Srđan BOŠNJAK
University of Belgrade
Faculty of Mechanical Engineering
Kraljice Marije 16, 11120 Belgrade 35, Serbia

Nebojša B. GNJATOVIĆ
University of Belgrade
Faculty of Mechanical Engineering
Kraljice Marije 16, 11120 Belgrade 35, Serbia

Ivan MILENOVIĆ
University of Belgrade
Faculty of Mechanical Engineering
Kraljice Marije 16, 11120 Belgrade 35, Serbia

E-mails: sbosnjak@mas.bg.ac.rs, ngnjatovic@mas.bg.ac.rs, imilenovic@mas.bg.ac.rs